Defence Science Journal, Vol. 71, No. 2, March 2021, pp. 137-145, DOI : 10.14429/dsj.71.15762

Comparative Analysis of Aerodynamic Characteristics of F16 and F22 Combat Aircraft using Computational Fluid Dynamics

Lohit Malik and Abhishek Tevatia*

Netaji Subhas University of Technology, New Delhi - 110 078, India
**E-mail: abhishek.tevatia@nsut.ac.in*

ABSTRACT

This paper presents the computational investigation of air flow over an aircraft at realistic speeds while demonstrating the importance of extending the existing analysis to the complete airplane and how pivotal it is in improving its in-flight performance. The study is done for F16 and F22 aircraft using ANSYS Fluent (19.2) to obtain pressure distribution, shear stress distribution and temperature variation on the complete surface of the aircraft. Since the front section of the aircraft is prone to direct initial impact of surrounding environment, this portion is also examined. Here, as the speed is doubled from Mach 1 to Mach 2, a rise in the value of all the three variables is noticed for the F16 aircraft, whereas the pressure distribution for F22 aircraft shows strange behaviour for the highest speed (Mach 2). On comparing the results over the whole surface, it is seen that F16 experiences smaller pressure (29% lower for Mach 1 and 30% for Mach 2), temperature (9.5% lower for Mach 1 and 30% for Mach 2) and shear stress relative to F22 and the stress shows a huge change (90% lower for Mach 1 and 83% for Mach 2). Results of the present study imply that the design of the aircraft highly influences its performance as the parameters discussed touch their limits.

Keywords: Lockheed Martin F16 raptor; General dynamics F22 flying Falcon; Computational fluid dynamics; Temperature and pressure variation; Shear stress distribution; Nosecone investigation

1. INTRODUCTION

Combat aircraft are principally used for in-air-fight against enemy aircraft. Apart from the pilot's skills and training, victory is highly dependent on various execution features including its firepower, thrust, highest altitude, maximum velocity and manoeuvrability in extreme situations; radar and comminution information also have significant impact. These features directly depend upon the parameters including airfoil shape, angle of attack (AoA), Reynolds number of the flow medium, pressure, shear stress, and temperature distribution on various parts of the aircraft[1-6]. This distribution is directly dependent on the design of aircraft. The manner in which the aircraft's body and its components including the wings and stabilizers are designed greatly influence the performance of the airplane. Along with this, the pilot's safety is dependent on the cockpit design. Hence, a detailed study of complete aircraft is crucial. Mostly the studies conducted by researchers[1-4,7-19] have provided us with detailed analysis of various airfoil shapes, how they control the forces generated on the wings and how performance can be improved by altering this shape, but the analysis of complete aircraft is not available.

With the fall in the pressure over the top surface of the NACA (National Advisory Committee for Aeronautics) airfoil 4412 a pressure change was noticed. This observation was confirmed at different AOA[1]. Khandwal & Singh[7] estimated lift and drag forces on airfoil using computational fluid dynamics (CFD) which were found to be in close agreement with the experimental results obtained by Abbott and Von Doenhoff[8]. It was confirmed experimentally that NACA 8321 produces the greatest lift force in comparison to other five airfoils being tested. These results were ascribed to the unique design of NACA 8321 airfoil that majorly comprised of thin cross-section and deep camber[2]. Sahu & Imam[9] proved the reliability of CFD by analysing the forces on the NACA 0012 airfoil for different combinations of aircraft speed and AOA that came out to be close to the experimentally obtained output[10-18]. On carrying out the CFD simulation of a wind turbine blade made up of the NACA 0012 airfoil for different AOA it was concluded that the velocity on the lower surface of the airfoil was higher than the velocity on its upper surface[19]. The above work was further extended by Patil & Thakare[3] for numerous Reynolds number ranging from 10000 to 800000 and the CFD results were very close to the ones obtained via experiments done at the Sandia National Laboratory. On doing the same study at Reynolds number 1000 and 5000 (relatively much smaller), it was noticed that Reynolds number and forces on the blade are directly proportional to each other. Sahin & Acir[4] performed experiments in a low-speed wind tunnel along with CFD to study the forces on the NACA0015 airfoil of a wind turbine at different AOA. It was concluded that till the 16-degree attack angle, both lift and drag coefficients rise but after this mark the lift coefficient falls while the drag coefficient dominates. Martynenko[21], *et al.* carried out the computational modelling of warhead transportation to estimate the maximum and most

Received : 28 April 2020, Revised : 25 January 2021
Accepted : 29 January 2021, Online published : 10 March 2021

dangerous load values due to forces at land operations and transportation by natural roads, aviation and water. These loads were used for numerically simulating the warhead using ANSYS, which helped analysing the operability and fatigue strength of the cartridge warhead using the calculations of the mean stresses and the amplitude fatigue stresses. On the other hand, Lee[22], *et al.* have recently developed an AOA command longitudinal control system for supersonic advanced trainer aircraft for improving its aerodynamic performance. Lei[23], *et al.* have numerically studied aerodynamic characteristics of variable-sweep morphing aircraft (VMA) where they investigated its characteristics at different AOA, aircraft speed, sweepback angle and elevation. In view of the fact that the prediction of afterbody and exhaust system aerodynamic drag are the key factors in the basic design of new combat aircraft, Zuccolo[24], *et al.* have employed reduced order models for predicting the performance of axisymmetric transonic afterbody and nozzle systems under the varied geometric degrees of freedom and aerodynamic conditions.

Precise and inexpensive CFD methods play a demanding role in the support of designing and operations of combat aircraft including other important investigations such as dynamic derivatives[25], flow around aircraft at high AOA[26], etc. However, prior to their deployment, these results need to be compared with and validated against the old school wind tunnel tests or the advanced flight-test data[27,28]. Cummings[29], *et al.* have demonstrated the superiority of CFD over the wind tunnel experiments under different conditions. Actually, the CFD has revolutionised the process of designing air vehicles, especially combat aircraft. It is no more a necessity to perform the physical tests of the concepts for verification. As a bonus, this method helps reduce the overall costs of a vehicle by eliminating the need of repair operations that were done to rectify the problems which can now be predicted and solved beforehand. Along with providing crucial design inputs, CFD also helps analysing the mechanisms governing the complex flows focused in the aerospace sector including carrier rockets, combat aircraft, missiles, transport airplanes, etc.[20]. Based on previously obtained results, it can be concluded that CFD is a better alternative to experimental testing in wind tunnels, especially in extreme conditions (explosion is one example). With the advancement in technologies giving rise to the ability to solve advanced algorithms in short time, studies were extended to the whole wing section. Focusing on an airplane wing, based on the CFD results, Prabhakar[5] concluded that there is a direct proportionality between the static pressure on the NACA 4412 airfoil and the AOA at the upper plane, lower plane and the leading edge of the wing whereas the dynamic pressure shows an inverse relation. Rao[22], *et al.* exploited CFD to analyse the performance characteristics of supersonic exhaust diffusers. As experimental testing at such harsh conditions is not possible, CFD turns out to be a solid and reliable method. The cockpit head load was calculated by Gupta & Rajput[6] at different elevations, aircraft speed and AOA in order to optimize the same to improve the airplane's performance. Only 5% difference was noticed between the CFD simulations and the experimental results obtained via flight tests. The computational technique i.e. CFD has eliminated the necessity to perform experiments and has transformed the design of aerial vehicles by a great extent in spite of the complex geometries associated along with the inclusion of weapons.

To the best of our knowledge, there are few studies on the shear stress and that too focused on a particular component of an airplane, but no effort has been made to examine the complete airplane. Keeping in mind this point and the need of analysis of complete aircraft for the reasons discussed here, the present work is dedicated to carry out a thorough analysis of the complete airplane comprising of all its elements with reference to the generated pressure, temperature and shear stress on the two airplanes, namely the F16 and the F22.

2. THEORETICAL ASPECT

The said problem is solved using the Navier-Stokes equations comprising of mass conservation equation, momentum equation and energy equation. As the speeds associated in the present work are higher than Mach 0.3, the density of the fluid medium, i.e. air changes with the pressure and hence the medium is considered compressible making this problem more complex than the incompressible one. The mass conservation equation, momentum equation and energy equation are respectively given as

$$\frac{D\rho}{Dt}+\nabla\cdot\left(\rho\vec{u}\right)=0 \tag{1}$$

$$\rho\frac{D\vec{u}}{Dt}=\nabla\cdot\vec{\sigma}+\rho\vec{g} \tag{2}$$

$$\frac{D}{Dt}\left(\rho e+\frac{1}{2}\rho\vec{u}\cdot\vec{u}\right)=-\nabla\cdot\vec{q}+\nabla\left(\vec{\sigma}\cdot\vec{u}\right)+\rho\vec{g}\cdot\vec{u} \tag{3}$$

Here, ρ, $\vec{u}$ and ∇ represent respectively the density of flow medium (Kg/m^3), the velocity vector, and the Del-operator. $\vec{\sigma}=\mu\left(\nabla\vec{u}+\left(\nabla\vec{u}\right)^T\right)-\left(p+\frac{2}{3}\mu\nabla\cdot\vec{u}\right)\mathrm{I}$ together with p as the mechanical pressure $\left(N/m^2\right)$ and μ as the coefficient of viscosity (kg/ms). e is the intrinsic energy per unit mass $\left(J/kg\right)$ while the heat flux vector is represented by $\vec{q}$.The effect of gravitational forces on the potential energy is governed by the term $\rho\vec{g}\cdot\vec{u}$ representing the change in potential energy due to the gravitational forces. The term $\nabla\left(\vec{\sigma}\cdot\vec{u}\right)$ represents the variation in energy as a result of internal stresses, and $\frac{1}{2}\rho\vec{u}\cdot\vec{u}$ depicts the kinetic energy.

3. CFD ANALYSIS

The two aircrafts chosen for this study are the Lockheed Martin F16 Raptor[31] and the General Dynamics F22 Flying Falcon[32]. The F-16 is a single engine multirole fighter aircraft. Use of relaxed static stability/ flight-by-wire control system makes it an agile aircraft. The F22 is a single seated all weather aircraft comes equipped with twin engines. Known for its air superiority and capability of ground attacks, electronic warfare and single intelligence comes in various versions namely F22, FA22, F22A, etc. The 3-D geometrical models of F-16 and F-22 are developed using Solid-works whose isometric views

are shown in Fig. 1 while the respective specifications have been compared in Table 1.

Table 1. Specifications of F16 and F22 Combat Aircraft

Specifications	F16 combat aircraft	F22 combat aircraft
Length	15 m	18.9 m
Wingspan	9.45 m	13.56 m
Thrust force	127530 N	155743 N
Maximum velocity	Mach 2.05	Mach 2
Highest altitude	15000 m	18288 m

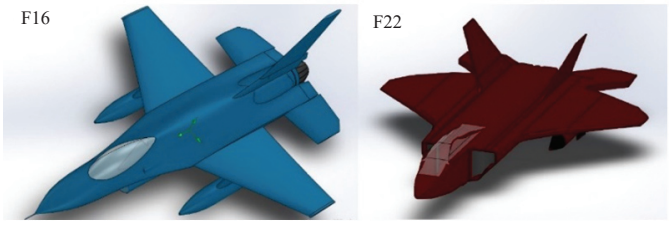

Figure 1. CAD models of the F16 and F22 aircraft.

3.1 Materials and Boundary Conditions

The altitude for flight test simulation has been taken as 1000 meter (1 km) which may facilitate practical performing of experiments in the future to validate the simulation results[6]. By fixing the altitude it becomes a requisite to calculate the exact values of the properties of air (the flow medium) such as pressure, temperature, density and viscosity at the taken elevation which will be required for setting up the boundary conditions. To get these values we use the standard atmospheric model according to which the pressure and temperature of air are only dependent on the altitude.

This model comprises of 3 regions divided based on the height from the sea level and the one we are concerned with is the troposphere (altitude< 11000 m). In this zone, the temperature decreases linearly, and the pressure reduces exponential with the height as formulated in the equations below.

The temperature T (in Celsius) is dependent on the elevation h (in meters) as:

$$T = 15.04 - (0.00649h) \tag{4}$$

The pressure P (in KPa) is dependent on the temperature T as:

$$P = 101.29\left[\frac{T+273.1}{288.08}\right]^{5.256} \tag{5}$$

Also, the density ρ (in Kg/m^3) is a function of both the temperature and the pressure according to the following relation:

$$\rho = \frac{P}{0.2869(T+273.1)} \tag{6}$$

The dynamic viscosity μ (in Ns/m^2) is given by:

$$\mu = \mu_0\left[\frac{T+2458.45}{T_0+2458.45}\right]^{1.5}\left[\frac{9T_0+3452.05}{9T+3452.05}\right] \tag{7}$$

where T is the temperature in Celsius and the value of the constant $T_0 = 15\,^\circ\text{C}$ and $\mu_0 = 1.7332\times10^{-5}\,Ns/m^2$. Substituting the value of the elevation h=1000 meters, we get $T = 8.55\,^\circ\text{C}$, P = 89.95 KPa, $\rho = 1.113$ Kg/m^3, and $\mu = 1.755\times10^{-5}\,Ns/m^2$

If we want to carry out similar study at a different altitude, the air properties and the boundary conditions will change accordingly which can be readily calculated using the relationships provided above.

Now we consider the material properties of the aircraft. In reality, the aircraft have a variety of materials including Steel, Aluminum, Composite, etc. employed at different parts depending on their vulnerability which helps in pulling down the overall force of friction. Since the exact distribution of the materials and their composition is not known, both the aircraft in the present study have been assigned an all-Aluminum body with the density of 2700 Kg/m^3. Doing so, we make a slight deviation from the actual values of the material properties such as coefficient of friction, Young's modulus, tensile strength, etc. Using this material, the larger value of coefficient of friction (approx. 1.4) is to be considered and it is the one that mainly contributes to the temperature and shear stress distribution. Hence, we anticipate higher values for the temperature and shear stress which would have been lower, if the actual material with the exact distribution was chosen. So, by choosing only Aluminum for the whole body we can say that we are playing safe by considering the worst-case scenario. On the other hand, there should not be a big difference in the actual and the studied pressure distribution because of its dependence on the force generated due to the drag and the area of contact which is independent of the material.

Several boundary conditions are already present in ANSYS Fluent as default, while the others have been incorporated in the following manner:

- Inlet:

Velocity Inlet: The inlet velocity has been taken as Mach 1 / 1.5 / 2 (depending on the study) perpendicular to the inlet plane. The turbulence intensity is set to 3 and 5.

- Outlet:

Pressure outflow: At the outlet the turbulence intensity is set to 3 and 5.

- Airplane wall:

The roughness constant and the roughness height have been set to default as 0.5 and 0, respectively.

- Operating temperature:

The temperature calculated for the altitude of 1000 meters using equation (4) comes out to be 8.55 °C.

- Operating pressure:

The pressure calculated using equation (5) comes out to be $8.995\times10^4\,N/m^2$, while the gauge pressure has been taken as zero.

- Angle of attack:

As we consider the situation when the aircraft attains a set speed and is horizontal, the AoA has been taken as zero.

The element size of the mesh is taken smaller in critical areas and larger in the non-critical regions. Results of such locally refined mesh are comparable to the results obtained by very fine mesh along with considerable reduction in the computation time. This way the results obtained will be closer

to the actual ones as it is expected that the to be discussed parameters will show the most changes in the finer mesh regions. Finally, the results obtained are discussed below in terms of pressure distribution, temperature rise, and shear stress distribution on the surface of the aircraft

4. RESULTS AND DISCUSSIONS

4.1 Pressure, Temperature and Shear Stress Distribution on F16

Figures 2(a) and 2(b) show the pressure distribution on the upper surface of the aircraft generated at the speeds of Mach 1 and Mach 2, respectively. As shown in Fig. 2(a), the nosecone, starting edges of the wings and the 3 stabilisers experience the maximum pressure (approx. 110000 Pa). The least pressure is on the middle portion of the wings (approx. 85000 Pa). For the remaining regions on the aircraft, the value of the pressure swings between these two values making it a non-uniform distribution on the surface of the aircraft. As the speed is doubled, the value of pressure in the earlier high-pressure regions (Fig. 2(a)) rises to 145000 Pa (Fig. 2(b)) which drops to 60000 Pa on moving across the wing axis. Such a drop in the value of pressure was also noticed by Prabhakar[5] while analysing the upper surface of an airplane wing. Focusing on the horizontal and vertical stabilisers, it can be observed that the pressure distribution is uniform irrespective of the speed but its value which is initially 90000 Pa at the speed of Mach 1 rises by 15000 Pa with the increment in the speed.

The temperature distribution (without consideration of product of combustion) in Fig. 2 (c) depicts that the engine and the exhaust areas are the high temperature zones (approx. 348 K) Rest of the body including the cockpit experiences relatively lower value (approx. 330 K) and has uniform distribution. Gupta & Rajput[6] also obtained such behaviour of temperature variation for their study of the cockpit at zero AoA. Due to a difference of Mach 0.2 in the speeds considered in their and our work, their work reports a relatively lower temperature of 320 K. As the speed is doubled, the red zones heat up to touch a temperature of 510 K while the remaining parts are found to be at 480K (Fig. 2(d)). This nature of rise is plausible as also seen in the work of Gupta & Rajput[6] at Mach 0.8. The F16 is designed to sustain engine temperatures as high as 1643K[33]. These red zones also develop on the missiles which is attributed to the high air resistance. Shear stress is generated

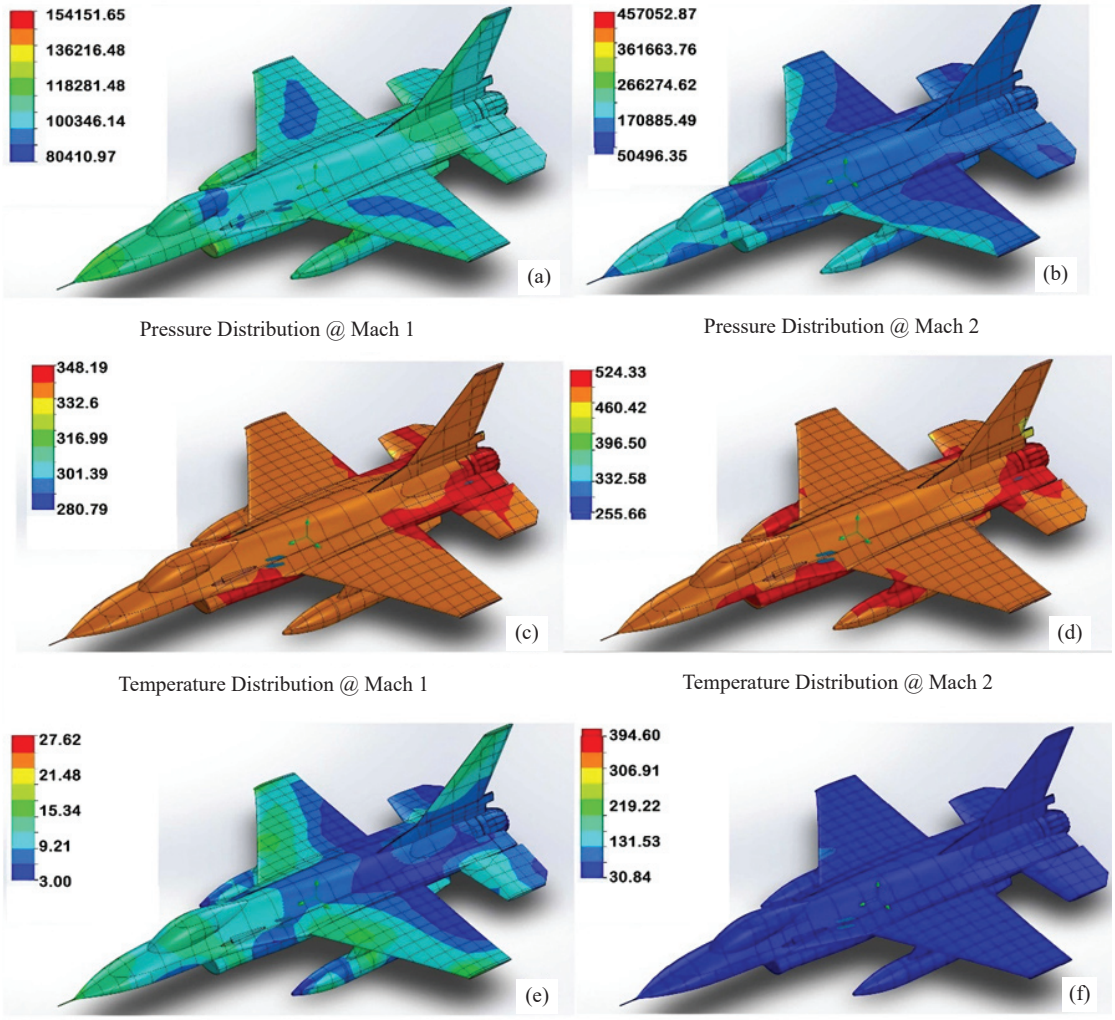

Figure 2. Computational fluid analysis of F16 aircraft.

due to the friction between the surface of the aircraft and the fluid flowing over it. This friction comes into play due to the viscous nature of the air. As shown in Fig. 2(e), the shear stress at nosecone, starting edges of the wings and the 3 stabilisers is relatively higher (approx. 14Pa) which is due to the initial contact of the resisting air. While on the remaining locations, this value is small (approx. 3Pa) as the air is not able to hold up at these positions.

On moving across the wing axis, it is observed that the value of the shear stress gradually decreases and approaches to zero at the end, as the air loses contact at the end of the wings. With the rise in the speed, the stress distribution turns very uniform, but the average value increases to 22Pa (Fig. 2(f)). To the best of our knowledge, no effort has been so far made to examine the shear stress distribution. The shear stress and the way it is distributed on the aircraft surface directly influences the drag force which indirectly controls the performance of the aircraft and more importantly its efficiency. This makes the study of shear stress distribution as important as the study of other parameters and hence, this work adds a new dimension to this field of study.

4.2 Pressure, Temperature and Shear Stress Distribution on F22

As seen from Figs. 3(a) and 3(b), the pressure is almost uniformly distributed all over the surface of F22, which suggests that the aircraft has an aerodynamic design. The average value of the pressure increments ranges from 100000 Pa to 200000 Pa as the speed doubles from Mach 1 to Mach 2. On observing of Fig. 3(a) careful, it can be concluded that at the end of the aircraft the pressure value is higher (approx. 180000 Pa). This may be due to the formation of a concentrated air channel between the two stabilisers. But as the speed is doubled, the pressure all over the surface increases and hence no such high-pressure areas are formed (Fig. 3(b)).

Exhaust and engine experience the highest temperature value (approx. 350K) followed by the front edge of the wings and the area surrounding the cockpit (approx. 340 K) which is attributed to the direct air impact (Fig. 3(c)). Gupta & Rajput[6] also noticed similar behaviour in their study of the cockpit. As mentioned earlier also, due to a slight difference in the speeds of their and our work (Mach 0.2) they observed temperature of about 320 K. The outer parts of the wings and the stabilizers

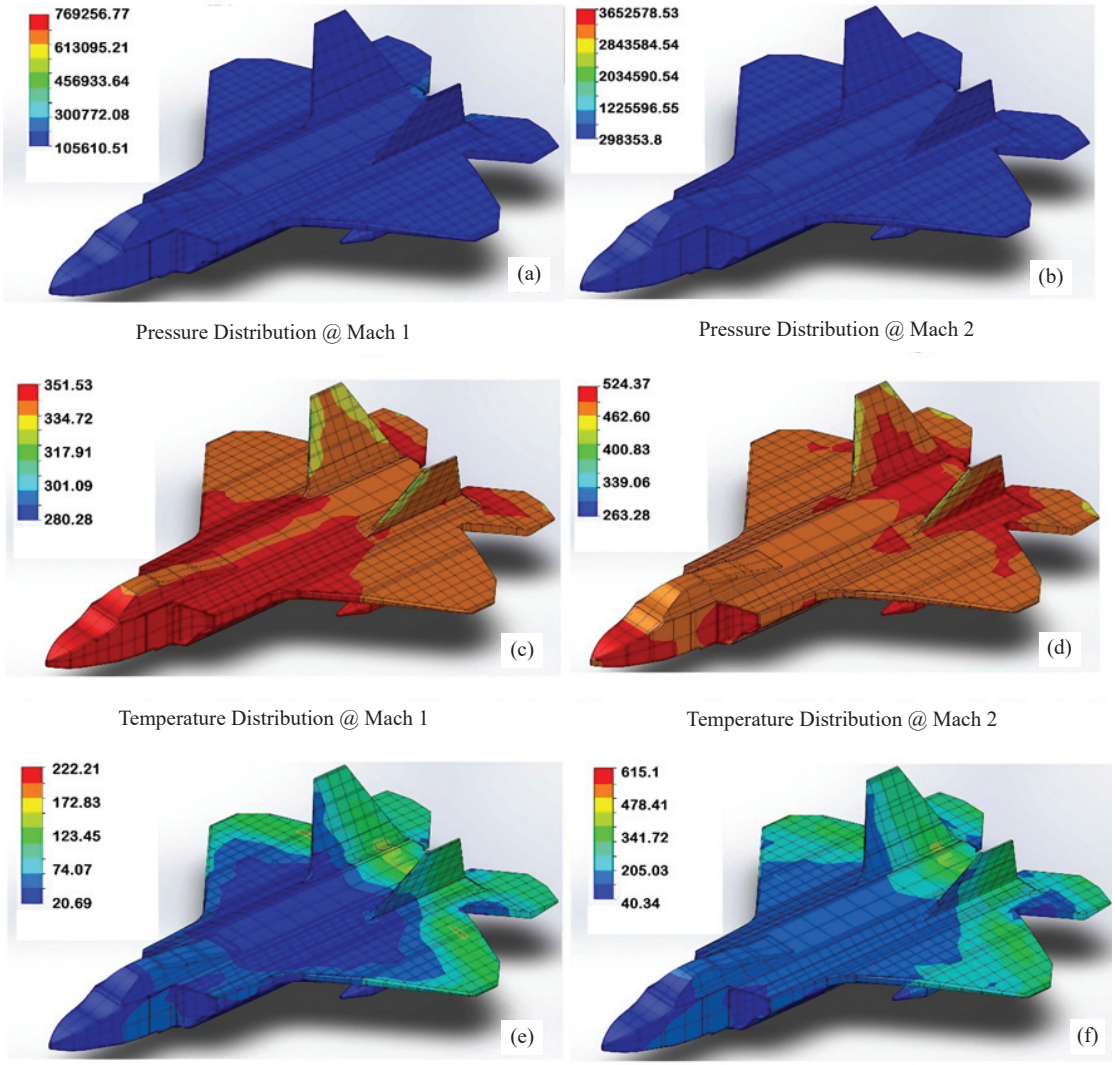

Pressure Distribution @ Mach 1

Pressure Distribution @ Mach 2

Temperature Distribution @ Mach 1

Temperature Distribution @ Mach 2

Shear Stress Distribution @ Mach 1

Shear Stress Distribution @ Mach 2

Figure 3. Computatioanl fluid analysis of F22 aircraft.

being away from the exhaust are cooler by 20 K. As seen in Fig. 3(d), with the rise in the speed, the temperature values peak at 520K around the engine, exhaust and the nose area. Due to heating up of the exhaust, heat flows up to the stabilizers to increase its temperature from 330 K to 450 K.

As shown in Fig. 3(e), the shear value is very small (approx. 12Pa) at the nosecone and the region between the cockpit and stabilisers. Entering the stabilisers section, the average value steadily increases to 110Pa. This is attributed to the high friction developed in this region due to the creation of three air channels, one channel between the two stabilisers and two channels between the wings and the stabilisers. With the rise in the speed, similar shear distribution is noticed but the value at the front section rises to 70Pa while at the stabilisers section it peaks to 350Pa (Fig. 3(f)).

4.3 Comparative Study of Highlighted Section of F16 and F22

So far, our focus was on the study of the complete aircraft at two different speeds of Mach 1 and Mach 2. Now, examining the highlighted section (Fig. 4) and an additional speed of Mach 1.5, a comparative study will be carried out in the forthcoming section for the variation of pressure, shear stress and temperature. Since we considered the situation when the aircraft attains a particular speed and moves horizontally, it is imperative to analyse the upper surface only. The investigations of the lower surface are important when the aircraft takes off or lands or there is a finite AoA. However, the lower surface carries more uniformity compared to the upper surface.

Figures 5, 6 and 7 show the variation of the quantities discussed above along the length of highlighted edge of F16 combat aircraft at different speeds. It is observed from Fig. 5 that profile for each speed is similar and almost comparable to Gaussian distribution. Initially, the pressure rises to a maximum value till the point which lies between 0.5 m to 1 m from the starting point, followed by a gradual fall and finally reaching a constant value roughly after the 1.5 m point. The position of the peaks shifts towards the right side of the graph, i.e. away from the starting point. Also, the pressure at every point rises with the increment in the speed.

As clearly seen in Fig. 6, the temperature at the same point approximately increases by 70K as the speed is consecutively increased. For the speeds of Mach 1 and Mach 1.5, the plots have very small slope (almost horizontal), i.e. the temperature at each point on the highlighted edge is almost the same. In case of Mach 2, the temperature initially rises by 10K till the 0.5 m point after which it is almost constant accompanied by a gentle fall after 1.25 m mark.

The value of shear stress at every point increases with the rise in the speed, as shown in Fig. 7, while at a particular speed the shear stress decreases as we move along the highlighted edge. Initially, this rate of fall is very small at Mach 1 which enhances steadily with the rise in the speed. At Mach 2, the value of shear stress is very high (approx. 50Pa) at the starting point and falls to (approx. 30Pa) as we move towards the end of the highlighted edge.

Figures 8, 9 and 10 depict the change in the discussed parameters along the highlighted length of F22 combat aircraft at different speeds. It is observed that there is not much variation in the pressure (Fig. 8) and temperature (Fig. 9), and these are almost constant for the speeds of Mach 1 and Mach 1.5. At Mach 2, the pressure plot is quite uneven with big variation in the pressure ordinates (approx. 70000Pa) with a sudden peak

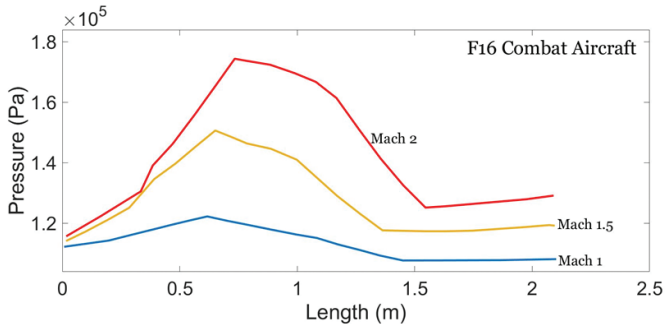

Figure 5. Pressure change at speeds of Mach 1, Mach 1.5 and Mach 2 on F16 combat aircraft.

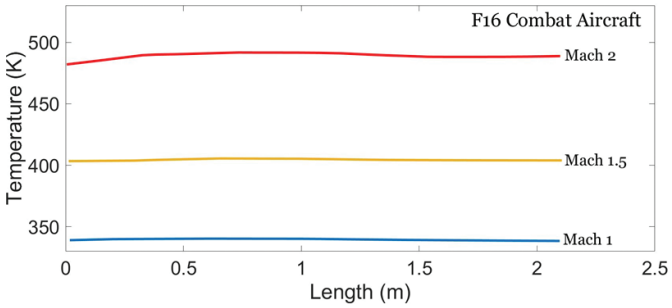

Figure 6. Temperature change at speeds of Mach 1, Mach 1.5 and Mach 2 on F16 combat aircraft.

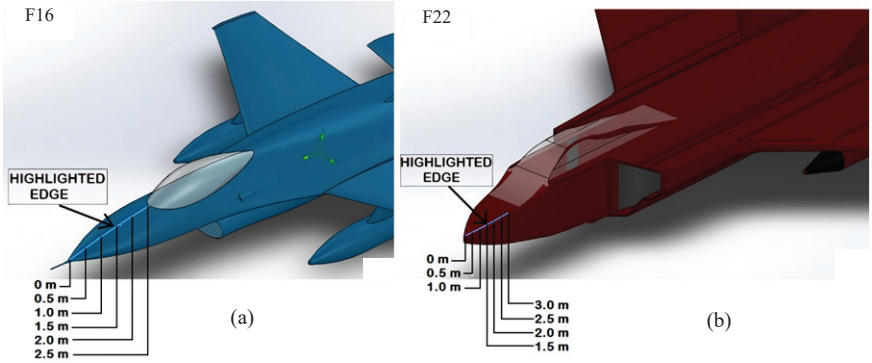

Figure 4. Highlighted edge of F16 and F22.

around the 1.5 m length mark. Comparably, in the temperature plot also, the variation in temperature values is relatively large (approx. 25K) for the speed of Mach 2. Here, the temperature initially rises and then starts falling steeply after length of 1.75 m.

As shown in Fig. 10, for shear stress, the graph falls and climbs almost linearly at the speeds of Mach 1 and Mach 1.5, respectively. For the speed of Mach 2, the value initially descends steeply and then suddenly peaks around length of 1.25 m followed by a portion of constant slope. Interestingly, for the speed of Mach 2, the difference in maximum and minimum shear stress ordinate values is big (approx. 40Pa) relative to other speeds just like the temperature and the pressure plots.

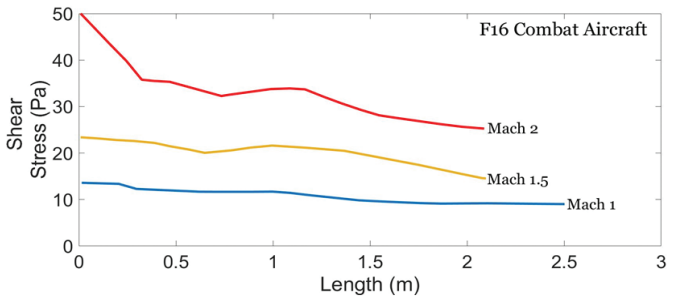

Figure 7. Shear Stress change at speeds of Mach 1, Mach 1.5 and Mach 2 on F16 combat aircraft.

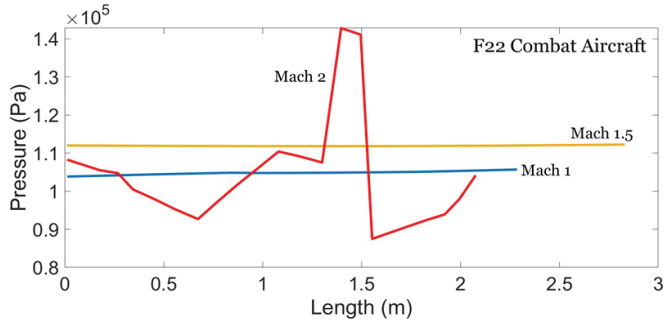

Figure 8. Pressure change at speeds of Mach 1, Mach 1.5 and Mach 2 on F22 combat aircraft.

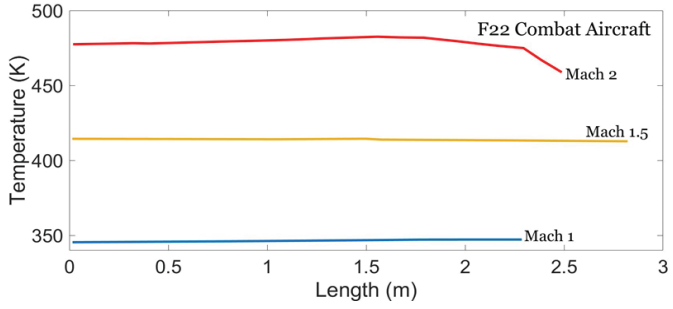

Figure 9. Temperature change at speeds of Mach 1, Mach 1.5 and Mach 2 on F22 combat aircraft.

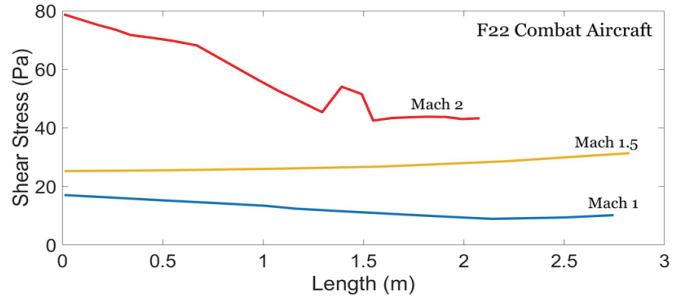

Figure 10. Shear Stress change at speeds of Mach 1, Mach 1.5 and Mach 2 on F22 combat aircraft.

4.4 Overall Comparison of F16 and F22 Aircraft

It is worth comparing the two aircraft according to the pressure obtained on the respective complete surfaces and so generated shear stress and temperature distributions.

Comparison of pressure generated: For the speed of Mach 1, going through the discussion of Figs. 2(a) and 3(a), it can be observed that the average pressure value of 100000 Pa on the F22 is slightly higher than the average pressure value of approximately 94000Pa on the F16. Hence, at the speed of Mach 1, overall F16 experiences lower pressure, but its distribution is not so uniform, whereas F22 is under slightly higher pressure but has uniform distribution all over the surface. Discussion of Figs. 2(b) and 3(b) done for the speeds of Mach 2 show that F22 experiences greater pressure with average value even higher than the maximum pressure on F16 surface.

Comparison of temperature distribution: After examining Figs. 2(c), 3(c), 2(d), and 3(d) it is seen that the differences between the maximum and minimum temperature values for the two aircraft are the same for the speed of Mach 1 and Mach 2. In case of Mach 1 (Figs. 2(c) and 3(c)), most of the front end of F22 lies in the red zone, unlike the case of F16. On increasing the speed, these red zones climb up to the stabilisers in the case of F22, while F16's stabilisers remain relatively cool. Hence, it can be stated that F16 has the innate ability to experience temperature jump for longer duration of time.

Comparison of shear stress distribution: Considering Figs. 2(e), 3(e), 2(f) and 3(f), it can be observed that the value of shear stress for F22 is much higher than the value for F16. For the speed of Mach 1, the average shear stress on F22 is approximately 6 times of the stress on F16 (Figs. 2(e) and 3(e)). As the speed is doubled, this factor reduces to 4, while the distribution for F16 turns uniform unlike in F22, where stress is higher at the front section (Figs. 2(f) and 3(f)). As lower value of the shear is desirable, F16 turns out to be a better candidate than F22.

5. CONCLUSIONS

Based on the results of CFD simulations we made interpretations and discussed the possible reasons for the obtained nature of pressure, shear stress and temperature distributions on the aircraft's surface. The comparison carried out under the same conditions reveals that F16 experiences lower pressure at Mach 1, but its distribution is not so uniform, whereas F22 is under slightly higher pressure but has uniform distribution all over the surface. At Mach 2, F22 experiences greater pressure with average value even higher than the maximum pressure on F16 surface. The temperature range experienced by both the aircraft are the same for the speeds corresponding to Mach 1 and Mach 2. At the speed of Mach 1, most of the front end of F22 lies in the red zone and these zones climb up to the stabilizers on increasing the speed, whereas F16's stabilizers remain relatively cool. The same temperature

range makes it easier to observe that area covered by the red zones in F22 is higher as compared to F16 which translates to higher temperatures on F22. For the speed corresponding to Mach 1, the shear stress for F22 is approximately 6 times than F16, which becomes 4 times at the doubled speed, while the shear distribution for F16 turns out to be uniform unlike in F22. Overall, the design of F16 is such that it can handle the temperature rise for longer time, experiences lower pressure and very small shear stress, making it a better aircraft in terms of usage.

REFERENCES

1. Gore, K.; Gote, A.; Govale, A.; Kanawade, A. & Humane, S. Aerodynamic analysis of aircraft wings using CFD. *Int. Res. J. Eng. Technol.,* 2018, **5**(6),639-44.
2. Sullivan, A. Aerodynamic forces acting on an airfoil. Physics Department, The College of Wooster, Ohio, USA. 2010 May 6.
3. Patil, BS. & Thakare, HR. Computational fluid dynamics analysis of wind turbine blade at various angles of attack and different Reynolds number. *Procedia Engineering*. 2015, **127**,1363-9.
   doi: 10.1016/j.proeng.2015.11.495
4. Şahin, İ. & Acir, A. Numerical and experimental investigations of lift and drag performances of NACA 0015 wind turbine airfoil. *Int. J. Mater., Mech. Manufacturing*, 2015, **3**(1), 22-25.
   doi: 10.7763/IJMMM.2015.V3.159
5. Prabhakar, A. A CFD analysis of static and dynamic pressure for NACA4412. *Int. J. Eng. Trends Technol.,* 2013, **4**(8), 3258-65.
6. Gupta, P. & Rajput, S.P. Optimised cockpit Heat load analysis using Skin temperature Predicted by CFD and Validation by thermal mapping to Improve the Performance of Fighter aircraft. *Def. Sci. J.,* 2015, **65**(1), 12-24.
   doi: 10.14429/dsj.65.7200
7. Kandwal, S. & Singh, S. Computational fluid dynamics study of fluid flow and aerodynamic forces on an airfoil. *Int. J. Eng. Technol.,* 2012, **1**(7), 1-8.
8. Abbott IH, Von Doenhoff AE. Theory of wing sections: including a summary of airfoil data. Courier Corporation; 2012 Apr 26.
9. Sahu, N.K. & Imam, M.S.; Analysis of transonic flow over an airfoil NACA 0012 using CFD. *IJISET.* 2015, **2**, 379-88.
10. Goorjian, P.M. & Guruswamy, G.P. Transonic unsteady aerodynamic and aeroelastic calculations about airfoils and wings. *Computers Structures,* 1988, **30**(4), 929-36.
11. Kaynak, U. & Flores, J. Advances in the computation of transonic separated flows over finite wings. *Computers Fluids*. 1989, **17**(2), 313-332.
12. Lien, F.S. & Kalitzin, G. Computations of transonic flow with the v2–f turbulence model. *Int. J. Heat Fluid Flow*. 2001, **22**(1), 53-61.
13. Lian, Y.; Steen, J.; Trygg-Wilander, M. & Shyy, W. Low Reynolds number turbulent flows around a dynamically shaped airfoil. *Computers and Fluids*, 2003, **32**(3), 287-303.
14. WANG, JF.& WU, YZ. Hierarchical Evolutionary Algorithms and Its Application in Transonic Airfoil Optimization in Aerodynamics. *Chinese J. Aeronautics*. 2003, **16**(1), 1-6. http://www.hkxb.net.cn/cja/2003/01/0001/ (Accessed on 2 April, 2020).
15. Vadillo, J.L.; Agarwal, R.K. & Hassan, A.A. Active control of shock/boundary layer interaction in transonic flow over airfoils. *In Computational Fluid Dynamics,* 2004 2006, (pp. 361-366), Springer, Berlin, Heidelberg.
16. Bourguet, R.; Braza, M. & Dervieux, A. Reduced-order modeling of transonic flows around an airfoil submitted to small deformations. *J. Comput. Phy.,* 2011, **230**(1), 159-84.
   doi: 10.1016/j.jcp.2010.09.019
17. C. Rumsey, Langley Research Center Turbulence Modeling Resource, NASA Langley Research Center, Hampton, VA, https://turbmodels. larc. nasa. gov/nasahump_val_sa. html [retrieved Sept. 2016] (2017).
18. Kuzmin, A. Non-unique transonic flows over airfoils. *Computers & Fluids*. 2012, **63**, 1-8.
19. Dash, A. CFD Analysis ofWind Turbine Airfoil at Various Angles of Attack. *IOSR J. Mech. Civ. Eng*.2016, **13**, 18-24.
   doi: 10.9790/1684-1304021824
20. Singh, K.P.; Mathur, J.S.; Ashok, V. & Chakraborty, D. Computational Fluid Dynamics in Aerospace Industry in India. *Def. Sci. J*., 2010, **60**(6), 639-652.
   doi: 10.14429/dsj.60.582
21. Martynenko, G.; Avramov, K.; Martynenko, V.; Chernobryvko, M.; Tonkonozhenko, A. & Kozharin, V. Numerical simulation of warhead transportation. *Defence Technology*, 2020.
   doi: 10.1016/j.dt.2020.03.005
22. Lee, D.; Sim, J.; Han, K.; Kim, C. & Koh, G.O. Angle-of-Attack Command Longitudinal Control for Supersonic Advanced Trainer Aircraft. *Int. J. Aeronautical Space Sci.,* 2020, 1-9.
   doi: 10.1007/s42405-020-00279-2
23. Lei, Y.; Zhang, D.; Zhang, Y. & Su, G. Numerical Study on Aerodynamic Characteristics of Variable-sweep Morphing Aircraft at Transonic Speeds. *IOP Conference Series: Mater. Sci. Eng.,* 2020, **751**(1), 012001.
   doi: 10.1088/1757-899X/751/1/012001.
24. Zuccolo, G.; Christie, R.; MacManus, D.; Goulos, I. & Martin, P. Low Order Models for Transonic Afterbody Aerodynamic Characteristics. In *AIAA Scitech* 2020 Forum. 2020, 1997.
   doi: 10.2514/6.2020-1997.
25. Da Ronch, A., Vallespin, D., Ghoreyshi, M. and Badcock, K.J. Computation of Dynamic Derivatives Using CFD. *AIAA paper*. AIAA-2010-4817]
26. Boelens, O.J. CFD analysis of the flow around the X-31 aircraft at high angle of attack. *Aerospace Sci. Technol.*, 2012, **20**(1), 38-51.
   doi: 10.1016/j.ast.2012.03.003
27. Fujii, K. Progress and future prospects of CFD in aerospace - Wind tunnel and beyond. *Progress Aerospace*

Sci., 2005, **41**(6), 455-470.
doi: 10.1016/j.paerosci.2005.09.001

28. Panagiotopoulos, E.E. & Kyparissis, S.D. CFD transonic store separation trajectory predictions with comparison to wind tunnel investigations. *Int. J. Eng.,* 2010, **3**(6), 538-553.
29. Cummings, R.M.; Liersch, C.M.; Schütte, A. & Huber, K.C. Aerodynamics and conceptual design studies on an unmanned combat aerial vehicle configuration. *Journal of Aircraft*, 2018, **55**(2), 454-474.
doi: 10.2514/1.C033808
30. Rao, M.S.; Javed, A. & Chakraborty, D. Numerical Characterisation of Supersonic Exhaust Diffusers. *Def. Sci. J.*, 2017, **67**(2), 219-223.
doi: 10.14429/dsj.67.9544
31. F16 Raptor specifications. https://www.lockheedmartin.com/en-us/products/f-16.html. (Accessed on 27 March, 2020)
32. F22 Flying Falcon specifications. https://www.lockheedmartin.com/en-us/products/f-22/f-22-specifications.html. (Accessed on 27 March, 2020)
33. F-16 combat aircraft general characteristics, features and flying controls. http://web.deu.edu.tr/atiksu/ana44/bilgi3.html. (Accessed on 27 March, 2020).

CONTRIBUTORS

Mr Lohit Malik is a third year Bachelor of Engineering student of Manufacturing Processes and Automation Engineering at NSIT, University of Delhi. He is a national level Award Winner of "Conserve My Campus" contest held by Schneider Electric Conzerv India Pvt. Ltd. in November 2009. He has published in Europhysics Letters of IOP Science (UK) and Optics and Laser Technology of Elsevier.
Contribution to the current study - Investigation, data analysis, data visualisation, and original draft writing.

Dr Abhishek Tevatia received PhD in the field of "Fatigue crack growth life prediction of metal matrix composites". Presently he is an Assistant Professor at the Department of Mechanical Engineering, NSUT, Dwarka, Delhi. His area of research and interest include Computer aided engineering, Advance computational modelling techniques, Finite element fatigue analysis of structures, Modelling of fatigue cracks in composite materials, Design sensitivity and uncertainty analysis.
Contribution to the current study - Conceptualisation, methodology, supervision, resources, review and editing of draft writing.